Article
Furin: A Potential Therapeutic Target for COVID-19

SARS-CoV-2

ACE2   Furin

Replication

Spike S1   Spike S2

SARS-CoV 658   A S Y H T V S L L - - - - R S T S Q K S I V A Y T M S L G
SARS-CoV-2 672   A S Y Q T Q T N S P R R A R S V A S Q S I I A Y T M S L G

Furin cleavage enhance receptor affinity and facilitate membrane fusion

Low-energy binding conformations of Diminazene bound to furin generated by molecular docking.

Host cells

Structure-based virtual ligand screening

H₂N

NH

N=N
N
H

NH

NH₂

Diminazene

IC₅₀= 5.42 ± 0.11 µM

Canrong Wu, Mengzhu Zheng, Yueying Yang, ..., Yonghui Zhang, Lixia Chen, Hua Li

zhouyirong@hust.edu.cn (Y.Z.)
zhangyh@mails.tjmu.edu.cn (Y.Z.)
syzyclx@163.com (L.C.)
li_hua@hust.edu.cn (H.L.)

HIGHLIGHTS
The unique "RRAR" motif in SARS-CoV-2-S is easily recognized and hydrolyzed by furin

A reason for high infectivity of SARS-CoV-2 is the furin cleavage site in Spike

Furin is a potential therapeutic target for COVID-19

Diminazene is a competitive inhibitor of furin, with an IC₅₀ of 5.42 ± 0.11 µM

Article

Furin: A Potential Therapeutic Target for COVID-19

Canrong Wu,[1,3] Mengzhu Zheng,[1,3] Yueying Yang,[2,3] Xiaoxia Gu,[1] Kaiyin Yang,[1] Mingxue Li,[2] Yang Liu,[2] Qingzhe Zhang,[1] Peng Zhang,[2] Yali Wang,[2] Qiqi Wang,[2] Yang Xu,[2] Yirong Zhou,[1,*] Yonghui Zhang,[1,*] Lixia Chen,[2,*] and Hua Li[1,2,4,*]

SUMMARY

COVID-19 broke out in the end of December 2019 and is still spreading rapidly, which has been listed as an international concerning public health emergency. We found that the Spike protein of SARS-CoV-2 contains a furin cleavage site, which did not exist in any other betacoronavirus subtype B. Based on a series of analysis, we speculate that the presence of a redundant furin cut site in its Spike protein is responsible for SARS-CoV-2's stronger infectious nature than other coronaviruses, which leads to higher membrane fusion efficiency. Subsequently, a library of 4,000 compounds including approved drugs and natural products was screened against furin through structure-based virtual screening and then assayed for their inhibitory effects on furin activity. Among them, an anti-parasitic drug, diminazene, showed the highest inhibition effects on furin with an IC_{50} of 5.42 ± 0.11 μM, which might be used for the treatment of COVID-19.

INTRODUCTION

A novel coronavirus (SARS-CoV-2) infectious disease broke out in the end of December 2019 and is still spreading rapidly, which has been listed as an international concerning public health emergency. As of August 17, 2020, a total of 21,777,834 patients have been diagnosed and 776,544 have died worldwide. This disease is caused by a novel coronavirus, which was named "2019-nCoV" by the World Health Organization, and the disease caused by 2019-nCoV was named COVID-19. 2019-nCoV, as a close relative of SARS-CoV, was classified as severe acute respiratory syndrome coronavirus 2 (SARS-CoV-2) by the International Committee on Taxonomy of Viruses on February 11, 2020.

Coronaviruses (CoVs) are mainly composed of four structural proteins, including Spike (S), Membrane (M), Envelope (E), and Nucleocapsid (N) (Bosch et al., 2003). Spike, a trimeric glycoprotein of CoVs, determines the diversity of CoVs and host tropism and mediates CoVs' binding to host cells surface-specific receptors and virus-cell membrane fusion (Lu et al., 2015). Current research found that SARS-CoV-2 belongs to the β-coronavirus genus and speculated that it may interact with angiotensin-converting enzyme 2 (ACE2) on the surface of human cells through Spike protein, thereby infecting human respiratory epithelial cell (Xu et al., 2020). Letko and Munster then identified the receptor for SARS-CoV-2 entry into human cells to be ACE2 (Letko et al., 2020).

Coronavirus Spike protein plays a key role in the early stages of viral infection, with the S1 domain responsible for receptor binding and the S2 domain mediating membrane fusion (Belouzard et al., 2009). The process of SARS-CoV infecting the host involves two indispensable cleaving processes, which affect the infectious capacity of SARS-CoV. First, Spike was cleaved into receptor-bound N-terminal S1 subunit and membrane-fusion C-terminal S2 subunit by the host proteases at S1/S2 cleavage site (such as type II transmembrane serine protease [TMPRSS2], cathepsins B and L) (Glowacka et al., 2011; Zhou et al., 2015). Second, after CoVs are endocytosed by the host, the lysosomal protease mediates cleavage of S2 subunit (S2′ cleavage site) and releases the hydrophobic fusion peptide to fuse with the host cell membrane (Kam et al., 2009).

Furin, a kind of proprotein convertases (PCs), is located in the *trans*-Golgi network and activated by acid pH (Feliciangeli et al., 2006). Furin can cleave precursor proteins with specific motifs to produce mature

proteins with biological activity. The first (P1) and fourth (P4) amino acids at the N terminus of the substrate cleavage site must be arginine "Arg-X-X-Arg ↓" (R-X-X-R, X: any amino acid, ↓: cleavage site). Kibler et al. demonstrated that the Spike protein S1/S2 and S2′ cleavage sites of the infectious bronchitis viruses (IBVs) Beaudette strain can be recognized by furin, which is a distinctive feature of IBV-Beaudette with other IBVs and has stronger infection ability (Tay et al., 2012; Yamada and Liu, 2009). Based on the characteristics of furin's recognition substrate sequence, some short peptide inhibitors have been developed, such as Decanoyl-Arg-Val-Lys-Arg-chloromethylketone (Dec-RVKR-CMK) and modified α1-antitrypsin Portland (α1-PDX). However, the non-specific and irreversible inhibitory effects on all members of the PC family limit their application (Henrich et al., 2003; Matsuyama et al., 2018). No small molecule inhibitor of furin with good effects and high specificity has been found so far.

The epidemiological observations showed that the infectious capacity of SARS-CoV-2 is stronger than that of SARS-CoV, so there are likely to be other mechanisms to make the infection of SARS-CoV-2 easier. We suppose the main possibilities as follows: first, SARS-CoV-2 RBD combining with ACE2 may have other conformations; second, the SARS-CoV-2 Spike protein can also bind to other receptors besides ACE2; third, Spike is more easily cleaved by host proteases and easily fused with host cell membrane. We compared the Spike proteins from three sources, SARS-CoV-2, SARS-CoV, and Bat-CoVRaTG13, and found that the SARS-CoV-2 virus sequence had redundant PRRA sequences. Through a series of analyses, this study proposes that one of the important reasons for the high infectivity of SARS-CoV-2 is a redundant furin cleavage site in its Spike protein. And through structure-based virtual ligand screening and in vitro enzyme-based assay, the anti-parasitic drug diminazene was found to show competitive inhibition on furin, with IC_{50} of 5.42 ± 0.11 μM.

RESULTS

Bioinformatics Analysis Reveals Furin Cut Site in Spike Protein of SARS-CoV-2

By sequence alignment of Spike protein sequence of SARS-CoV-2 with its highly homologous sequences, it was found that the Spike cleavage site of SARS-CoV-2 possessed four redundant amino acids—PRRA, and these were not found in those of high-homology sequences, thus forming a furin-like restriction site as RRAR (Figures S1 and S2). Through prediction in ProP 1.0 Server, it is true that the sequence was easily digested by furin (Figure S3). To explore the evolution of this sequence, we used the BLASTp method to find 1,000 homologous Spike sequences with homology from 100% to 31%, which are all from β-CoVs. Multiple sequence alignments were performed on these thousands of Spike sequences. One sequence was selected from each highly homologous class (homology greater than 98.5%) for further sequence alignment, and about 155 sequences were finally selected. A homologous multiple sequence alignment was performed on these 155 sequences, and then a phylogenetic tree was constructed (Figure 1). As shown in the phylogenetic tree, the Spike of SARS-CoV-2 exhibited the closest linkage to those of Bat-SL-CoV and SARS-CoV, and far from those of MERS-CoV, HCoV-HKU1, and HCoV-OC43. In general, most of the Spike proteins in α-CoVs do not contain a furin cleavage site, but it is very popular in γ-CoVs' Spike protein, and with or without furin cleavage site are common in β-CoVs (Millet and Whittaker, 2015). We systematically analyzed the four subtypes of β-CoVs and found that only SARS-CoV-2 in the subtype B β-CoVs contains the furin cleavage site, and most of the subtype A β-coronaviruses contain the furin restriction site.

We performed furin digestion site prediction on the sequence of each type of coronavirus Spike through online software. It was found that all Spike with a SARS-CoV-2 Spike sequence homology greater than 40% did not possess a furin cleavage site (Figure 1, Table 1), including Bat-CoV RaTG13 and SARS-CoV (with sequence identity as 97.4% and 78.6%, respectively). The furin cleavage site "RRAR" of SARS-CoV-2 is unique in its family, rendering by its unique insert of "PRRA." The furin cleavage site of SARS-CoV-2 is unlikely to have evolved from MERS, HCoV-HKU1, and so on. From the currently available sequences in databases, it is difficult for us to find the source. Perhaps there are still many evolutionary intermediate sequences waiting to be discovered.

By analysis of the SARS-CoV-2 Spike protein sequence, we found that most of features are similar to those of SARS-CoV. It has an N-terminal signal peptide and is divided into two parts, S1 and S2. Among them, S1 contains N-terminal domain and receptor-binding region and S2 is mainly responsible for membrane fusion. The C-terminal region of S2 is S2′, containing a fusion peptide, heptad repeat 1, heptad repeat 2, and a transmembrane domain (Figure 2A). There are two cleavage sites between S1 and S2′, named CS1 and CS2. However, there are some differences in these two cleavage sites.
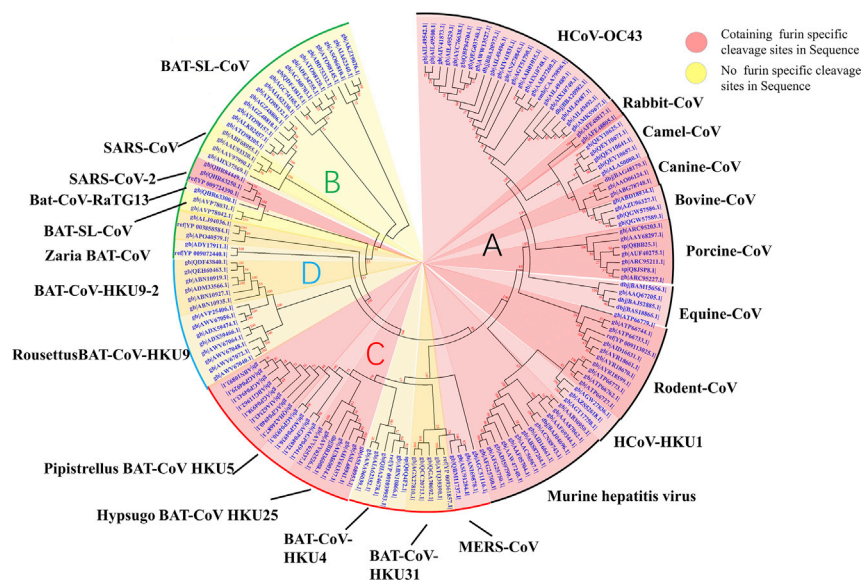
Figure 1. Evolutionary Relationships of Taxa

The evolutionary history was inferred using the neighbor-joining method. The bootstrap consensus tree inferred from 500 replicates is taken to represent the evolutionary history of the taxa analyzed. Branches corresponding to partitions reproduced in less than 50% bootstrap replicates are collapsed. The evolutionary distances were computed using the Poisson correction method and in the units of the number of amino acid substitutions per site. The analysis involved 155 amino acid sequences. All positions containing gaps and missing data were eliminated. There are a total of 711 positions in the final dataset. Evolutionary analyses were conducted in MEGA7. Red shading means containing cleavage site in sequences and yellow shading means no cleavage site in sequences. All sequences are from β-coronavirus, and the four subtypes are marked in different outline colors.

Unlike SARS-CoV, SARS-CoV-2 contains polybasic amino acids (RRAR) at the CS1 digestion site, and trypsin digestion efficiency will be significantly improved here (Belouzard et al., 2009). More importantly, as mentioned above, this site can be recognized and cleaved by the furin enzyme. The cleavage of Spike protein promotes structural rearrangements of RBD for the adaptation to receptor, thus increasing the affinity (Walls et al., 2019). More importantly, the digestion of Spike is indispensable for membrane fusion of S2 part (Kirchdoerfer et al., 2016). In this case, the cleavage efficiency of the SARS-CoV-2 Spike protein cleavage is significantly higher than that of SARS-CoV, and the SARS-CoV-2 Spike protein could be cleaved during the process of biosynthesis, which has been verified by a recent research (Walls et al., 2020) (Figure 2B). The receptor affinity and membrane fusion efficiency of SARS-CoV-2 would be significantly enhanced when compared with that of SARS-CoV. The membrane fusion of SARS-CoV-2 Spike protein is more likely to occur on the host cell plasma membrane. This may explain the strong infectious capacity of SARS-CoV-2. So, the development of furin inhibitors may be a promising approach to block its transmissibility.

Homology Modeling and Protein-Protein Docking Calculation

In our previous studies (Wu et al., 2020), both SARS and SARS-CoV-2 Spike RBD structures have been docked with human ACE2 to calculate their binding free energy. In that time, the complex structure of SARS-CoV-2 RBD with ACE2 was not available. Its energy was calculated based on the homology model generated from SARS_RBD-ACE2 complex. The binding free energy between the SARS-CoV-2 Spike RBD and human ACE2 was -33.72 KCal mol^{-1} and that between SARS-CoV Spike RBD and ACE2 was -49.22 KCal mol^{-1}. This means the binding affinity between SARS-CoV-2 Spike and ACE2 is weaker than that of SARS Spike. During this manuscript preparation, the structure of SARS-CoV-2 Spike RBD-ACE2 complex was disclosed (Wang et al., 2020). Based on this new real structure of SARS-CoV-2 Spike RBD-ACE2 complex, we re-did the calculation and found that the binding free energy between SARS-CoV-2 Spike RBD and ACE2 was -50.13 kcal mol^{-1} (Figure S4). This means the binding affinity between SARS-CoV-2 Spike and ACE2 is slightly stronger than that of SARS Spike. By inspecting the crystal structure of SARS-CoV-2 RBD-ACE2 complex and SARS RBD-ACE2 complex, one can find that one key loop of SARS-CoV-2 RBD in the complex interface had very different conformation compared with that of SARS RBD and previously modeled SARS-CoV-2 RBD (Figure S5).

Description	Accession No.	CS1 Sequence	Furin Score[a]	Identity[b]
SARS-CoV-2	QHR63250.1	NSPRRAR/SV	0.620	100%
Bat-CoV-RaTG13	QHR63300.1	QTQTNSR/SV	0.151	97.4%
Bat-SL-CoV	AVP78042.1	HTASILR/ST	0.170	80.3%
SARS-CoV	ABF68955.1	QLTPAWR/IY	0.117	76.0%
Bat-CoV HKU5	AGP04941.1	PSARLAR/SD	0.697	37.1%
MERS-CoV	QBM11737.1	LTPRSVR/SV	0.563	35.0%
Rat-CoV	AFG25760.1	TAHRARR/SV	0.879	36.3%
MHV	ABS87264.1	TSHRARR/SI	0.861	36.9%
HCoV-HKU1	AGT17758.1	SSRRKRR/GI	0.744	36.8%
Rodent-CoV	ATP66727.1	TARRKRR/AL	0.795	37.3%
β-CoV sp	AYR18670.1	ATRRAKR/DL	0.753	35.9%
Equine-CoV	BAS18866.1	TARRQRR/SP	0.815	37.1%
Porcine-CoV	ARC95227.1	TSLRSRR/SL	0.758	36.1%
Bovine-CoV	QGW57589.1	TKRRSRR/AI	0.780	37.5%
Canine-CoV	ABG78748.1	TQRRSRR/SI	0.832	37.1%
Camel-CoV HKU23	ALA50080.1	IDRRARR/FT	0.718	36.5%
Rabbit-CoV HKU14	AFE48805.1	TLQPSRR/AI	0.629	37.7%
Human-CoV OC43	AMK59677.1	KTRRSRR/AI	0.720	36.8%

Table 1. Furin Cleavage Probability of Spike Sequence Homology
[a]Scores are predicted by ProP 1.0 Server. Scores above 0.5 mean furin cleavable.
[b]Identities compared with SARS-CoV-2 Spike protein.

To further explore the possible mechanism of furin cleaving SARS-CoV-2 Spike, we perform protein-protein docking for furin and Spike. We already built a homology model of SARS-CoV-2 Spike in our recently published article (Wu et al., 2020). SARS-CoV-2 Spike structure was built by using the SARS-CoV Spike structure as the template (PDB: 5X58) (Yuan et al., 2017). To verify the accuracy of homologous modeling, we aligned the computational structure of the SARS-CoV-2 Spike that modeled from the SARS-CoV spike with its cryoelectron microscopic (cryo-EM) structure (PDB: 6VXX) that was just solved and released when this manuscript was being revised and submitted (Walls et al., 2020). The computational model of the SARS-CoV-2 Spike showed a Cα root-mean-square deviation of 1.571 Å on the overall structure compared with the SARS-CoV-2 Spike cyro-EM structure, demonstrating a very subtle difference.

By superimposing the SARS-CoV Spike with the SARS-CoV-2 Spike, we can find that the major conformation differences between two structures are the RBD domain, Arg685/677 loop region (furin/trypsin/TMPRSS2 cut site), and S2 loop region just after fusion peptide (Figure 3A). The trypsin/TMPRSS2 cut sites of both SARS-CoV and SARS-CoV-2 Spikes were disordered and missing from the original cryo-EM structures possibly due to their flexibility and lack of electro density; we built this region by modeling software. The "PRRA" inserting in this region of SARS-CoV-2 apparently generates the more flexible loop region and accessible cut site for protease. We performed protein-protein docking by setting SARS-CoV-2 Spike furin cleavage loop as the receptor and furin active pocket as the ligand (Figure 3B). The protein-protein docking results showed that furin acidic/negative active pocket can be well fitted onto the SARS-CoV-2 Spike basic/positive S1/S2 protease cleavage loop with low energy (−18.43 KCal mol^{-1}). This implies that the extra "PRRAR" loop of SARS-CoV-2 Spike renders it more fragile to the protease. And this may allow this site to be cut during the maturation, efficiently enhancing the infection efficiency.
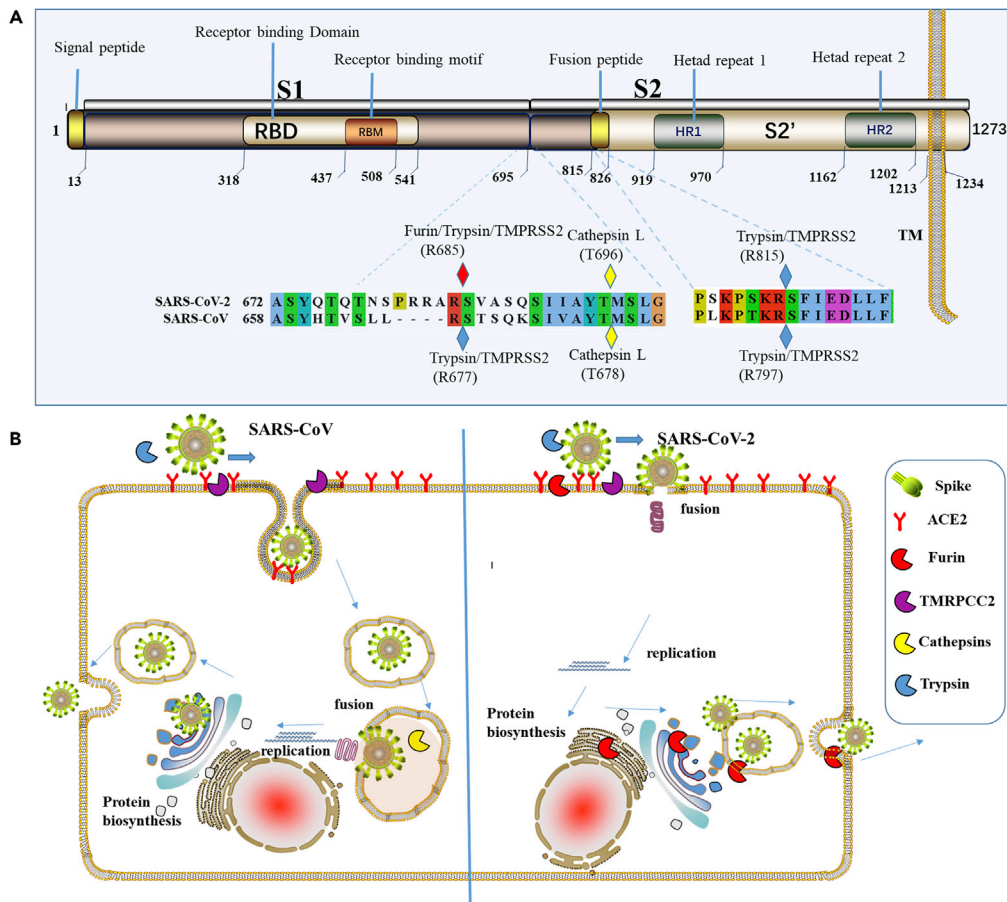
Figure 2. Analysis of SARS-CoV-2 Spike Protein and Its Membrane Fusion Mode

(A) Sequence analysis of Spike protein in SARS-CoV-2. It contains an N-terminal signal peptide, S1 and S2. S1 contains N-terminal domain and receptor-binding region. S2 is mainly responsible for membrane fusion. The C-terminal region of S2 is S2', and it contains a fusion peptide, HR1, HR2, and a transmembrane domain. The amino acid sequence numbers of every domain are annotated below them. Cleavage sites contained in SARS-CoV and SARS-CoV-2 are marked by rhombus.

(B) A schematic diagram of the process of SARS-CoV and SARS-CoV-2-infecting host cells. Those proteases are presented by sector in different colors. Furin can cleave Spike in the process of viral maturation.

Validation of RRAR Motif as the Furin Cleavage Site

By the online ProP 1.0 Server software prediction, we proposed that furin can cleave the RRAR sequence, but the cleavage efficiency of this sequence has not been determined. To measure the cleavage efficiency, we performed a set of experiments to determine the Michaelis-Menten constant (K_m) and limiting rate (V_{max}) of furin using fluorogenic peptide substrate, Boc-RRAR-AMC (Table 2, Figure 7A). Kinetic parameters were also determined by using the second AMC substrate containing the authentic cleavage motif Arg-Val-Arg-Arg (Table 2, Figure 7A). Boc-RRAR-AMC has a similar K_m value toward furin compared with Boc-RVRR-AMC. Using this substrate, a 2-fold higher hydrolysis efficiency was observed as demonstrated by the limiting rate, indicating that the "RRAR" motif is easily recognized by furin and quickly hydrolyzed.

Virtual Ligand Screening of Furin Target and Validation

Structure-based virtual ligand screening method was used to screen potential furin protein inhibitors through ICM 3.7.3 modeling software (MolSoft LLC, San Diego, CA) from a ZINC Drug Database (2,924 compounds), a small in-house database of natural products (including reported common antiviral components from traditional Chinese medicine) and derivatives (1,066 compounds), and an antiviral compounds library containing 78 known antiviral drugs and reported antiviral compounds. Compounds with lower
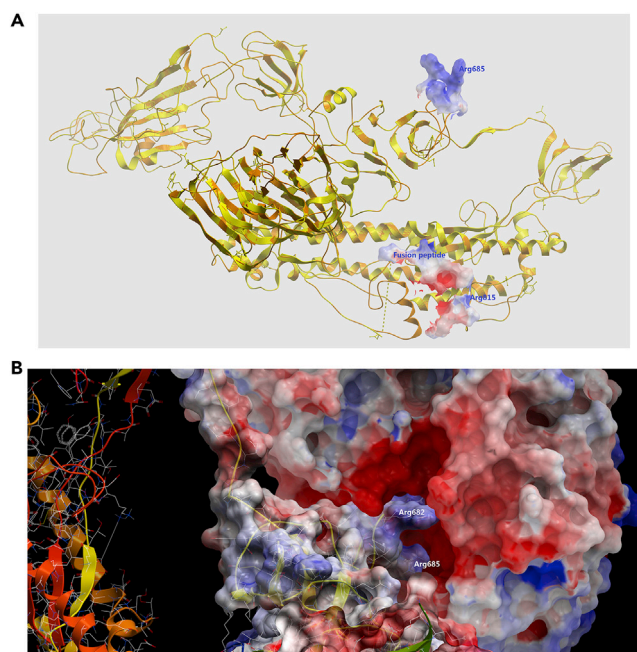
Figure 3. Protein-Protein Docking Model of SARS-CoV-2 Spike with Furin

(A) Superimposition of SARS-CoV Spike and SARS-CoV-2 Spike. Two S1/S2 protease cleavage sites and fusion peptide were shown as electrostatic surface mode.

(B) Furin was docked onto the putative furin cut site (Arg685) of SARS-CoV-2 Spike. Both domains are shown as electrostatic surface mode.

calculated binding energies (being expressed with scores and mfscores) are considered to have higher binding affinities with the target protein.

The screening results for the ZINC Drug Database (Table S1) showed that anti-tumor drugs aminopterin, fludarabine phosphate, and irinotecan; antibacterial drugs sulfoxone, lomefloxacin, and cefoperazone; antifungal drug hydroxystilbamidine; anti-parasitic drug diminazene; antiviral drug valganciclovir; hepato-protective drug silybin; folic acid supplement folinic acid; etc., have higher binding affinity to furin with mfscores lower than −100 or scores lower than −30.

Here, we show one example of screen hits, diminazene, which was predicted to bind in the active site of furin with low binding free energy. In the generated docking model, diminazene was well fitted into the binding pocket of the substrate and adopted similar conformation as substrate analogous inhibitor MI-52 in PDB model PDB: 5JXH (Dahms et al., 2016), and occupied two arms' position of MI-52 (Figure 4A). Asp154, Asp258, and Asp306 were predicted to form three hydrogen bonds with imine groups of compounds (Figure 4B). It looks like that diminazene mimics at least two arginines. Weak hydrophobic interaction of His194, Leu227, the backbone of Trp254, and Asn295 with the compound may further stabilize its conformation.

Another example was anticancer drug imatinib. It was also predicted to bind in the active site of furin. In the generated docking model, imatinib was fitted well in the binding pocket and occupied the top two arms'

Substrate	Km (μM)	Vmax (RFU/min)
Boc-RRAR-AMC	20.72 ± 1.30	221.5 ± 3.81
Boc-RVRR-AMC	19.16 ± 0.93	111.1 ± 1.45

Table 2. Kinetic Parameters of Furin with Different Substrates
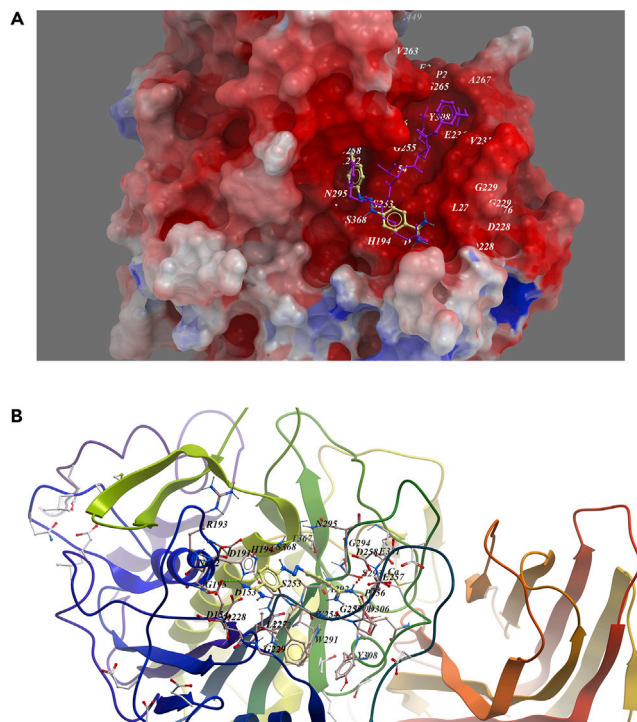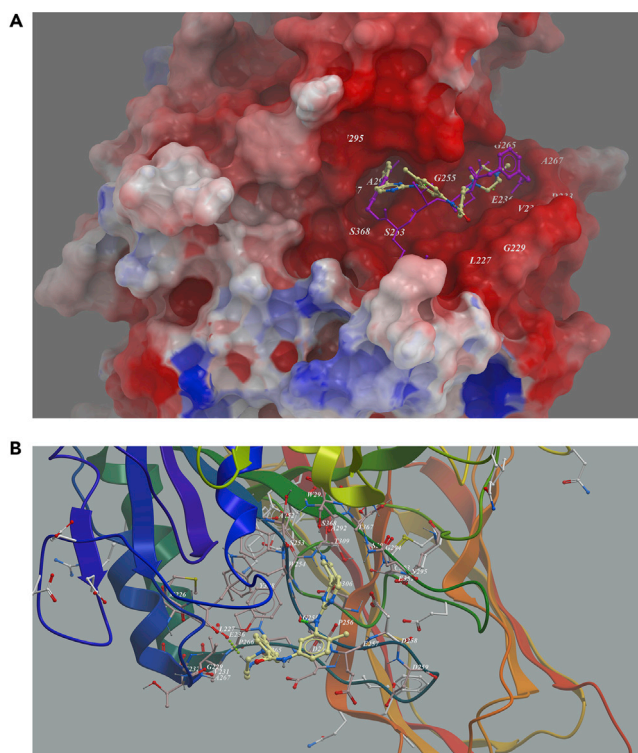
Figure 4. Low-Energy Binding Conformations of Diminazene Bound to Furin Generated by Molecular Docking
(A) Diminazene was fitted well in the active pocket of human furin, and furin was shown as electrostatic surface model.
Diminazene (yellow) was overlapped with substrate analog inhibitor MI-52 (purple).
(B) Detailed view of diminazene binding in the active pocket of furin.

position of MI-52 (Figure 5A). Two hydrogen bonds were predicted to form between the compound with Glu236 and Gly255. Weak hydrophobic interaction between Val231, Pro256, Trp254, and Gly294 and the compound was found (Figure 5B).

For the natural products (Table S2), a series of compounds with antiviral and anti-inflammation effects, such as (−)-epigallocatechin gallate (ECCG) and theaflavin 3,3′-di-O-gallate from *Camellia sinensis*, biorobin from *Ficus benjamina*, andrographolide and 14-deoxy-11,12-didehydroandrographiside from *Andrographis paniculata*, 2β,30β-dihydroxy-3,4-seco-friedelolactone-27-lactone from *Viola diffusa*, phyllaemblicin G7 from *Phyllanthus emblica*, and xanthones kouitchenside J and kouitchenside F from *Swertia kouitchensis* exhibited potential high binding affinity to furin protein (mfscores < −100).

EGCG was predicted to bind in the active site of furin, as imatinib; it occupied the top two arms' position of MI-52 (Figure 6A). Two hydrogen bonds were predicted to be formed between the compound with Asp258 and Ala292. Weak hydrophobic interactions between Pro256, Trp254, and Gly294 and the compound were predicted (Figure 6B).

The database of 78 antiviral drugs including compounds already on the market and currently undergoing clinical trials to treat SARS-CoV-2 infections was further screened. The results were shown in Table S3. DNA topoisomerase II inhibitor suramin treating hand-foot-and-mouth disease exhibited the highest affinity with furin (mfscore = −190.406). Indinavir, tenofovir alafenamide, tenofovir disoproxil, isoproxil, dolutegravir, boceprevir, and telaprevir may also have high binding affinity with furin.

To validate the finding of virtual ligand screening, the recombinant human furin was expressed in HEK-293-GnTI and purified. We tested the furin enzyme inhibitory effect of all the available compounds with a final concentration of 100 μM (Table S4). Among them, the anti-parasitic drug diminazene showed an inhibition ratio over 95%, and other compounds like aminopterin, methotrexate, and silybin showed inhibition ratio over 70%. Among them, diminazene showed significantly dose-dependent inhibition on furin protease,
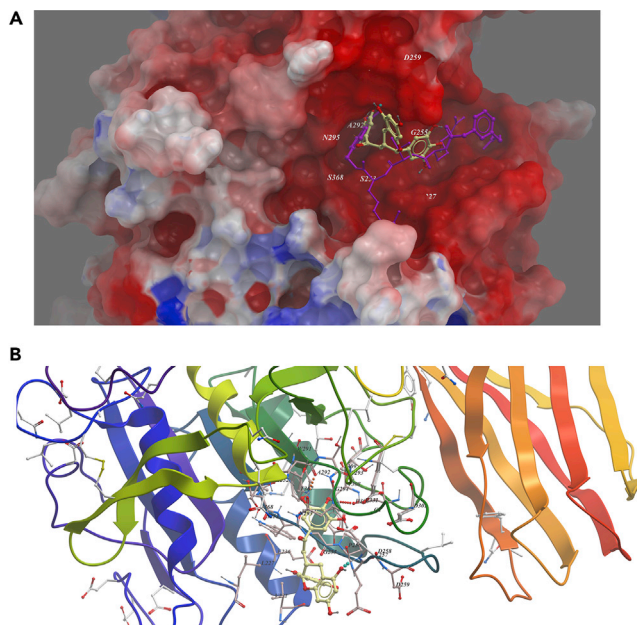
Figure 5. Low-Energy Binding Conformations of Imatinib to Furin Generated by Molecular Docking
(A) Imatinib was fitted well in the active pocket of human furin, and furin was shown as electrostatic surface model.
Imatinib (yellow) was overlapped with substrate analog inhibitor MI-52 (purple).
(B) Detailed view of Imatinib binding in the active pocket of furin.

with IC_{50} value of 5.42 ± 0.11 μM (Figure 7B). Enzyme kinetics has also been measured to explore its mode of inhibition. As shown in Figures 7C and 7D, diminazene displayed a competitive inhibition mechanism characterized by dose-dependent increase in Km and little effects on Vmax (Table 3).

DISCUSSION

Our previous study (Wu et al., 2020) analyzed the amino acid composition of the RBD domain of the ACE2 receptor of SARS-CoV-2 and Bat-CoVRaTG13. We found that several key amino acids determining binding were mutated in SARS-CoV-2, which are more similar to that of SARS-CoV. The calculation results showed that in the same conformation as the SARS-CoV protein, the binding free energy of SARS-CoV-2 and ACE2 receptors was a little higher, but this result cannot fully explain the epidemiologically high contagion, so we speculate that (1) the RBD domain of SARS-CoV-2 may have other conformations, (2) there may be other receptors, and (3) there are other mechanisms that enhance infectivity. During the preparation of this manuscript, the cryo-EM structure of SARS-CoV-2 Spike was solved (Walls et al., 2020). Comparing the structure of SARS-CoV-2 with the Spike structure of SARS-CoV, combined with biophysical detection, they found that SARS-CoV-2 binds more strongly to cellular ACE2 receptors (Walls et al., 2020). Further-more, the just disclosed crystal structure of SARS-CoV-2 RBD-ACE2 complex showed a distinct con-formational change in the key loop of complex binding interface. And the binding free energy calculation indicated a slightly stronger binding for SARS-CoV-2 RBD compared with that for SARS RBD. These results confirm our supposition that the conformational change of the RBD domain of SARS-CoV-2 leads to stron-ger binding. However, stronger receptor binding still cannot fully explain the more infectious problem of SARS-CoV-2.

So we put forward the following hypotheses: (1) SARS-CoV-2 can also bind to other receptors, (2) the lung may not be the earliest infection site, and (3) SARS-CoV-2 is easier to be cut and more easily fuses with cell membranes. As published in the Pubmed database, researchers performed RNA sequencing analysis on

Figure 6. Low-Energy Binding Conformations of ECCG to Furin Generated by Molecular Docking

(A) ECCG was fitted well in the active pocket of human furin, and furin was shown as electrostatic surface model. ECCG (yellow) was overlapped with substrate analog inhibitor MI-52 (purple).

(B) Detailed view of ECCG binding in the active pocket of furin.

tissue samples from 95 individuals' 27 different tissues. The results showed that ACE2 protein was highly expressed in the small intestine and duodenum, but the expression level in lung tissue is low (Figure S6). However, we analyzed the expression of furin and found that it is distributed in various organs with little difference in expression level. Combined with the possible infection mechanism of SARS-CoV-2, the widespread distribution of furin increases the SARS-CoV-2 infection of other organs. The possibility of other organ attack is consistent with the multiple symptoms observed in clinic of COVID-19.

Based on these three conjectures, we compared the Spike sequences from SARS-CoV-2, SARS-CoV, and Bat-CoVRaTG13 and found an extra "PRRA" insert near the S1/S2 cleavage site. During the preparation of this manuscript, there were also a few studies reporting this potential furin site. Xin Li et al. proposed the possible furin cleavage sites (Li et al., 2020), but their classification of β-coronavirus was unclear, and their speculation that the packaging mechanism of SARS-CoV-2 was similar to HIV and Ebola viruses was insufficiently supported. This site was also reported in another article and aligned with several other human coronaviruses (Coutard et al., 2020). In our research, furin score of this site predicted by ProP 1.0 server was 0.62, and the feasibility of furin cutting in this site of the Spike protein of SARS-CoV-2 was evaluated by protein-protein docking and free energy calculation. More importantly, we simulated the recognition and hydrolysis of RRAR sequence by furin through hydrolysis of the fluorescent substrate Boc-RRAR-AMC and found that the substrate Boc-RRAR-AMC can be effectively recognized and cleaved by furin, and its hydrolysis efficiency was higher than Boc-RVRR-AMC, a known substrate of furin.

We systematically analyzed the four subtypes of β-CoV and found that SARS-CoV-2 was the only one in the subtype B β-CoV that contains the furin cleavage site, whereas most of the subtype A contains the furin restriction site (Figure 1). We aligned 1,000 Spike sequences and found that all Spikes with sequence homology greater than 40% of SARS-CoV-2 Spike did not have a furin cleavage site, but its possible evolutionary source cannot be found currently, and more novel viruses are needed to be discovered. Very recently, a new closely related virus RmYN02 containing PAA at the CS1 of the S protein has been reported, but it also had no furin cleavage sites (Zhou et al., 2020).

The "PRRA" insert and subsequent arginine (R) constitute an RRAR sequence that could be recognized and cleaved by furin-like proteases, which may be the reason why SARS-CoV-2 infection is stronger than
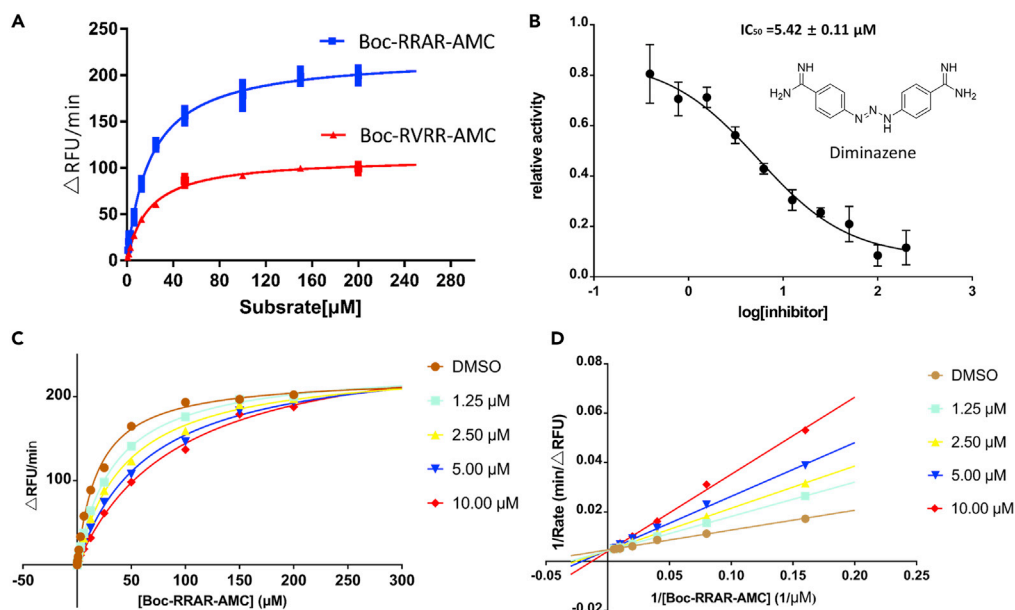
Figure 7. *In Vitro* **Enzymatic Characterization of Recombinant Human Furin Protease and Enzyme Inhibition Assay**

(A) Substrate saturation profiles for furin. Representative plots of the initial rate (Vi in △RFU/min) versus the amounts of fluorogenic substrate Boc-RVRR-AMC or Boc-RRAR-AMC. The *Vmax* and *Km* were determined by fitting the experimental data to a pseudo-first-order rate curve yielding the computed value and the best fit curve.

(B) Dose response inhibition of furin activity by diminazene.

(C) Substrate saturation profiles for furin at a range of concentrations of diminazene.

(D) Lineweaver-Burk double-reciprocal representation of the Boc-RRAR-AMC saturation profiles for furin at a range of concentrations of Boc-RRAR-AMC.

SARS-CoV. What's more, we performed a homologous alignment and phylogenetic analysis of the SARS-CoV-2 sequence and found that "PRRA" insert did not appear in any other close relatives of SARS-CoV-2, indicating that this insert was completely novel in this genus of virus. The existence of such a motif may allow Spikes to be cut into S1 and S2 by furin-like proteases before maturity, which provides S1 with the flexibility to change the conformation to better fit the host receptor. According to studies of Simmons et al., overexpression of furin can increase the activity of SARS-CoV Spike, but it will not cause Spike to be cleaved (Simmons et al., 2011). This is consistent with our prediction.

Furthermore, Glowacka et al. and Simmons et al. have demonstrated that SARS-CoV Spikes can be activated by cleavage in two ways, including proteolytic activation by cathepsins B and L in host cells (Simmons et al., 2005). In addition, SARS-CoV Spike can be activated by TMPRSS2 cleavage on the host cell surface (Glowacka et al., 2011). As we can see in Figure 2B, the Spike protein of SARS-CoV-2 can be cleaved at multiple stages, which greatly increases the efficiency of fusion. Markus et al. demonstrated that the CS1 of the S protein of SARS-CoV-2 was easily cleaved in the host cell, and they mentioned that TMPRSS2 plays an important role in the cleavage of CS2 (Hoffmann et al., 2020). It is likely that the virus will fuse with the cell in the cell plasma membrane and release the genome into cells. In addition, the receptor affinity of the cleaved Spike is also greatly enhanced (Parka et al., 2016).

According to our study, furin-like proteases may be potential drug targets for anti-SARS-CoV-2 treatment. At present, some peptide inhibitors have been developed and have good effects (Dahms et al., 2018; Dahms et al., 2017). To search for potential inhibitors of furin-like proteases, we screened potential compounds from a ZINC drug database (2,924 compounds), a small in-house database of natural products (1,066 compounds), and existing antiviral drugs library (78 compounds) with furin by virtual ligand screening. We found that a series of anti-tumor, antibacterial, antiviral, anti-parasitic, and hepatoprotective drugs may have high binding affinity to furin.

Concentration of Diminazene (µM)	Km (µM)	Vmax (RFU/min)
DMSO	19.84 ± 1.02	226.0 ± 2.8
1.25	33.28 ± 0.84	234.7 ± 1.6
2.5	43.09 ± 2.25	236.7 ± 3.7
5.0	61.86 ± 4.02	248.9 ± 5.5
10.0	76.31 ± 7.32	252.1 ± 9.0

Table 3. Kinetic Parameters of Furin with Different Concentrations of Diminazene

To validate the results of the virtual ligand screening, we tested the furin enzyme inhibitory effect of all the available compounds with a final concentration of 100 µM. It was found that some of these compounds did exhibit certain inhibitory effects on furin, such as aminopterin, silybin, diminazene, methotrexate, lomefloxacin, imatinib, tenofovir, disoproxil, etc. Among them, diminazene showed the strongest inhibitory activity with an IC_{50} of 5.42 ± 0.11 µM. It was found to be a competitive inhibitor by analyzing its enzyme kinetics characteristic on furin. Diminazene is probably occupied the substrate-binding pocket of furin, which is consistent with the result of molecular docking. Diminazene might be a drug candidate for the treatment of COVID-19 by inhibiting furin, or can at least serve as a lead compound to guide the development of novel furin inhibitors for the treatment of COVID-19. What's more, combined administration of furin inhibitors targeting different SARS-CoV-2 proteases may be an effective therapeutic strategy. The furin inhibitor here might open a new avenue for the treatment of COVID-19. Further experiments to verify its efficiency both *in vitro* and *in vivo* will be carried out in our future studies.

Limitation of the Study

A total of 1,000 SARS-CoV-2 Spike homologous sequences were searched through BLASTp method, but the Spike proteins of the newly discovered viruses, such as RmYN02 and pangolin-CoV, were not included in the database. So several Spike protein sequences were not analyzed in this study.

Resource Availability

Lead Contact

Further information and requests for resources should be directed to the Lead Contact, Hua Li (li_hua@hust.edu.cn).

Materials Availability

Materials and the information used for the experiments are available upon reasonable request.

Data and Code Availability

All data used in the study are included in this publication. The present research did not use any new codes.

METHODS

All methods can be found in the accompanying Transparent Methods supplemental file.

SUPPLEMENTAL INFORMATION

Supplemental Information can be found online at https://doi.org/10.1016/j.isci.2020.101642.

AUTHOR CONTRIBUTIONS

H.L. and C.W conceived the story. H.L., L.C., C.W., M.Z., Y.Y., Y. Zhang, and Y. Zhou analyzed the data; interpreted the results; and contributed to critical discussions. H.L., L.C., C.W., M.Z., and Y.Y drafted the manuscript, and all authors contributed to revising the manuscript.

DECLARATION OF INTERESTS

Authors declare no conflict of interest and no competing financial interest.

REFERENCES

Belouzard, S., Chu, V.C., and Whittaker, G.R. (2009). Activation of the SARS coronavirus Spike protein via sequential proteolytic cleavage at two distinct sites. Proc. Natl. Acad. Sci. U S A 106, 5871–5876.

Bosch, B.J., van der Zee, R., de Haan, C.A., and Rottier, P.J. (2003). The coronavirus Spike protein is a class I virus fusion protein: structural and functional characterization of the fusion core complex. J. Virol. 77, 8801–8811.

Coutard, B., Valle, C., de Lamballerie, X., Canard, B., Seidah, N.G., and Decroly, E. (2020). The Spike glycoprotein of the new coronavirus 2019-nCoV contains a furin-like cleavage site absent in CoV of the same clade. Antivir. Res 176, 104742.

Dahms, S.O., Arciniega, M., Steinmetzer, T., Huber, R., and Than, M.E. (2016). Structure of the unliganded form of the proprotein convertase furin suggests activation by a substrate-induced mechanism. Proc. Natl. Acad. Sci. U S A 113, 11196–11201.

Dahms, S.O., Hardes, K., Steinmetzer, T., and Than, M.E. (2018). X-ray Structures of the proprotein convertase furin bound with substrate analogue inhibitors reveal substrate specificity determinants beyond the S4 pocket. Biochemistry 57, 925–934.

Dahms, S.O., Jiao, G.S., and Than, M.E. (2017). Structural studies revealed active site distortions of human furin by a small molecule inhibitor. ACS Chem. Biol. 12, 1211–1216.

Feliciangeli, S.F., Thomas, L., Scott, G.K., Subbian, E., Hung, C.H., Molloy, S.S., Jean, F., Shinde, U., and Thomas, G. (2006). Identification of a pH sensor in the furin propeptide that regulates enzyme activation. J. Biol. Chem. 281, 16108–16116.

Glowacka, I., Bertram, S., Muller, M.A., Allen, P., Soilleux, E., Pfefferle, S., Steffen, I., Tsegaye, T.S., He, Y., Gnirss, K., et al. (2011). Evidence that TMPRSS2 activates the severe acute respiratory syndrome coronavirus Spike protein for membrane fusion and reduces viral control by the humoral immune response. J. Virol. 85, 4122–4134.

Henrich, S., Cameron, A., Bourenkov, G.P., Kiefersauer, R., Huber, R., Lindberg, I., Bode, W., and Than, M.E. (2003). The crystal structure of the proprotein processing proteinase furin explains

its stringent specificity. Nat. Struct. Biol. 10, 520–526.

Hoffmann, M., Kleine-Weber, H., Schroeder, S., Krüger, N., Herrler, T., Erichsen, S., Schiergens, T.S., Herrler, G., Wu, N.H., Nitsche, A., et al. (2020). SARS-CoV-2 cell entry Depends on ACE2 and TMPRSS2 and is blocked by a clinically proven protease inhibitor. Cell 181, 271–280.

Kam, Y.W., Okumura, Y., Kido, H., Ng, L.F., Bruzzone, R., and Altmeyer, R. (2009). Cleavage of the SARS coronavirus Spike glycoprotein by airway proteases enhances virus entry into human bronchial epithelial cells in vitro. PLoS One 4, e7870.

Kirchdoerfer, R.N., Cottrell, C.A., Wang, N., Pallesen, J., Yassine, H.M., Turner, H.L., Corbett, K.S., Graham, B.S., McLellan, J.S., and Ward, A.B. (2016). Pre-fusion structure of a human coronavirus Spike protein. Nature 531, 118–121.

Letko, M., Marzi, A., and Munster, V. (2020). Functional assessment of cell entry and receptor usage for SARS-CoV-2 and other lineage B betacoronaviruses. Nat. Microbiol. 5, 562–569.

Li, X., Duan, G.Y., Zhang, W., Shi, J.S., Chen, J.Y., Chen, S.M., Gao, S., and Ruan, J.S. (2020). A furin cleavage site was discovered in the S protein of the 2019 novel coronavirus. Chin. J. Bioinformatics 18, 1–4.

Lu, G., Wang, Q., and Gao, G.F. (2015). Bat-to-human: spike features determining 'host jump' of coronaviruses SARS-CoV, MERS-CoV, and beyond. Trends Microbiol. 23, 468–478.

Matsuyama, S., Shirato, K., Kawase, M., Terada, Y., Kawachi, K., Fukushi, S., and Kamitani, W. (2018). Middle east respiratory syndrome coronavirus Spike protein is not activated directly by cellular furin during viral entry into target cells. J. Virol. 92, e00683–18.

Millet, J.K., and Whittaker, G.R. (2015). Host cell proteases: critical determinants of coronavirus tropism and pathogenesis. Virus Res. 202, 120–134.

Parka, J.E., Lib, K., Barlana, A., Fehrc, A.R., Perlmanb, S., McCray, P.B., and Gallagher, T. (2016). Proteolytic processing of middle east respiratory syndrome coronavirus Spikes expands virus tropism. Proc. Natl. Acad. Sci. U S A 113, 12262–12267.

Simmons, G., Bertram, S., Glowacka, I., Steffen, I., Chaipan, C., Agudelo, J., Lu, K., Rennekamp, A.J., Hofmann, H., Bates, P., et al. (2011). Different host cell proteases activate the SARS-coronavirus Spike-protein for cell-cell and virus-cell fusion. Virology 413, 265–274.

Simmons, G., Gosalia, D.N., Rennekamp, A.J., Reeves, J.D., Diamond, S.L., and Bates, P. (2005). Inhibitors of cathepsin L prevent severe acute respiratory syndrome coronavirus entry. Proc. Natl. Acad. Sci. U S A 102, 11876–11881.

Tay, F.P., Huang, M., Wang, L., Yamada, Y., and Liu, D.X. (2012). Characterization of cellular furin content as a potential factor determining the susceptibility of cultured human and animal cells to coronavirus infectious bronchitis virus infection. Virology 433, 421–430.

Walls, A.C., Park, Y.-J., Tortorici, M.A., Wall, A., McGuire, A.T., and Veesler, D. (2020). Structure, function and antigenicity of the SARS-CoV-2 spike glycoprotein. Cell 181, 281–292.

Walls, A.C., Xiong, X., Park, Y.-J., Tortorici, M.A., Snijder, J., Quispe, J., Cameroni, E., Gopal, R., Dai, M., Lanzavecchia, A., et al. (2019). Unexpected receptor functional mimicry elucidates activation of coronavirus fusion. Cell 176, 1026–1039.

Wang, Q., Zhang, Y., Wu, L., Niu, S., Song, C., Zhang, Z., Lu, G., Qiao, C., Hu, Y., Yuen, K.-Y., Wang, Q., Zhou, H., Yan, J., and Qi, J. (2020). Structural and functional basis of SARS-CoV-2 entry by using human ACE2. Cell 181, 894–904.

Wu, C.R., Liu, Y., Yang, Y.Y., Zhang, P., Zhong, W., Wang, Y.L., Wang, Q.Q., Xu, Y., Li, M.X., Li, X.Z., et al. (2020). Analysis of therapeutic targets for SARS-CoV-2 and discovery of potential drugs by computational methods. Acta Pharm. Sin. B 10, 766–788.

Xu, X., Chen, P., Wang, J., Feng, J., Zhou, H., Li, X., Zhong, W., and Hao, P. (2020). Evolution of the novel coronavirus from the ongoing Wuhan outbreak and modeling of its Spike protein for risk of human transmission. Sci. China Life Sci. 63, 457–460.

Yamada, Y., and Liu, D.X. (2009). Proteolytic activation of the Spike protein at a novel RRRR/S motif is implicated in furin-dependent entry,

syncytium formation, and infectivity of coronavirus infectious bronchitis virus in cultured cells. J. Virol. *83*, 8744–8758.

Yuan, Y., Cao, D., Zhang, Y., Ma, J., Qi, J., Wang, Q., Lu, G., Wu, Y., Yan, J., Shi, Y., et al. (2017). Cryo-EM structures of MERS-CoV and SARS-CoV Spike glycoproteins reveal the dynamic

receptor binding domains. Nat. Commun. *10*, 15092.

Zhou, H., Chen, X., Hu Li, J., Song, H., Liu, Y.R., Wang, P.H., Liu, D., Yang, J., Holmes, E.C., Hughes, A.C., et al. (2020). A novel bat coronavirus reveals natural insertions at the S1/S2 cleavage site of the Spike protein and a possible

recombinant origin of HCoV-19. bioRxiv. https://doi.org/10.1101/2020.03.02.974139.

Zhou, Y., Vedantham, P., Lu, K., Agudelo, J., Carrion, R., Nunneley, J.W., Barnard, D., Pohlmann, S., McKerrow, J.H., Renslo, A.R., et al. (2015). Protease inhibitors targeting coronavirus and filovirus entry. Antivir. Res. *116*, 76–84.

Supplemental Information

Furin: A Potential Therapeutic

Target for COVID-19

Canrong Wu, Mengzhu Zheng, Yueying Yang, Xiaoxia Gu, Kaiyin Yang, Mingxue Li, Yang Liu, Qingzhe Zhang, Peng Zhang, Yali Wang, Qiqi Wang, Yang Xu, Yirong Zhou, Yonghui Zhang, Lixia Chen, and Hua Li

Supplementary information

Furin, a potential therapeutic target for COVID-19

Canrong Wu,[a,1] Mengzhu Zheng,[a,1] Yueying Yang,[b,1] Xiaoxia Gu,[a] Kaiyin Yang,[a] Mingxue Li,[b] Yang Liu,[b] Qingzhe Zhang,[a] Peng Zhang,[b] Yali Wang,[b] Qiqi Wang,[b] Yang Xu,[b] Yirong Zhou,[a,*] Yonghui Zhang,[a,*] Lixia Chen,[b,*] Hua Li[a,b,*,2]

[a]*Hubei Key Laboratory of Natural Medicinal Chemistry and Resource Evaluation, School of Pharmacy, Tongji-Rongcheng Center for Biomedicine, Tongji Medical College, Huazhong University of Science and Technology, Wuhan 430030, China*
[b]*Wuya College of Innovation, Key Laboratory of Structure-Based Drug Design & Discovery, Ministry of Education, Shenyang Pharmaceutical University, Shenyang 110016, China*

[1] These authors contributed equally to this work.
[2] Lead Contact.

*Corresponding author: Hua Li, Lixia Chen, Yonghui Zhang & Yirong Zhou
E-mail: li_hua@hust.edu.cn (H. Li)
   syzyclx@163.com (L. Chen)
   zhangyh@mails.tjmu.edu.cn (Y. Zhang)
   zhouyirong@hust.edu.cn (Y. Zhou),

Transparent Methods

Homology Spike protein blast and sequence alignment.

The Spike protein of (GB: QHR63250.1) was downloaded from NCBI nucleotide database. The protein sequence were aligned with whole database using BLASTp to search for homology viral Spike protein (Alogorithm parameters, Max target sequences: 1000, Expect threshold: 10). Multiple-sequence alignment was conducted in BLASTp online and analysis with DNAMAN and Jalview. The evolutionary history was inferred using the Neighbor-Joining method in MEGA 7 software package. The percentage of replicate trees in which the associated taxa clustered together in the bootstrap test was determined by 500 replicates. The Spike protein sequence analyses were conducted in snapgene view.

Furin cleavage site prediction

The prediction of furin cleavage sites were carried out in ProP 1.0 Server (http://www.cbs.dtu.dk/services/ProP/).

Compounds database

Approved drug database was from the subset of ZINC database, ZDD (ZINC drug database) containing 2924 compounds (Irwin et al., 2012). Natural products database was constructed by ourselves, containing 1066 chemicals separated from traditional Chinese herbals in own lab and natural-occurring potential antiviral components and derivatives. Antiviral compounds library contains 78 known antiviral drugs and reported antiviral compounds through literature search.

Homology modeling and molecular docking

Corresponding homology models predicted by Fold and Function Assignment System server for each target protein were downloaded from Protein Data Bank (www.rcsb.org). Alignment of two protein sequences and subsequent homology modeling were performed by bioinformatics module of ICM 3.7.3 modeling software on an Intel i7 4960 processor (MolSoft LLC, San Diego, CA). For the structure-based virtual screening, ligands were continuously resiliently made to dock with the target that was represented in potential energy maps by ICM 3.7.3 software, to identify possible drug candidates. 3D

compounds of each database were scored according to the internal coordinate mechanics (Internal Coordinate Mechanics, ICM) (Abagyan et al., 1994). Based on Monte Carlo method, stochastic global optimization procedure and pseudo-Brownian positional/torsional steps, the position of intrinsic molecular was optimized. By visually inspecting, compounds outside the active site, as well as those weakly fitting to the active site were eliminated. The software adopted two kind of scoring system. One is ICM score, which is based on the empirical function of predicted physical interaction, calculated according to seven parameters, including ligand-target hydrogen bonding interactions,internal force-field energy of the ligand, desolvation energy of hydrogen bond donor-acceptor,entropy loss due to conformational differences upon ligand binding, polar and non-polar solvation energychanges upon ligand binding,electrostatic energyand hydrophobic free energy (Neves et al., 2012). Another is mfscore, it is a potential of mean force score and provides an independent score of the strength of ligand-receptor interaction. It is a measure of statistical probability of interaction between the ligand and the receptor. It examines interatomic distances of the docked interaction, and compares that to existing interactions available in PDB (Muegge et al., 1999).

Compounds with Scores less than -30 or mfScores less than -100 (generally represents strong interactions) have priority to be selected. Protein-protein docking procedure was performed according to the ICM-Pro manual.

Expression and purification of furin

The detailed procedures for expression and purification of human furin (UNIPROT ID P09958) refer to previous work with some modifications (Dahms et al., 2018). Briefly, the sequence encoding human furin amino acids 23-574 was cloned into PEGMan vector with N-terminal secretion signal peptide and C-terminal His tag. The expressed plasmid was transfected in HEK293-GnTI cells using polyethylenimine transfection reagent, and the transfected cells were cultured in a 10 cm plate with 10 mL of DMEM (Invitrogen) containing 10% bovine calf serum (HyClone, GE Healthcare) overnight. The medium was changed to 10 mL of freeStyle 293 Expression Media (Thermo Fisher Scientific), and the

cells were cultured for another 72 h. The conditioned medium was collected and centrifuged at 4500 g for 20 min. The supernate protein was dialysis against 25 mM Tris, pH 8.0, 250 mM NaCl, 5 mM $CaCl_2$ overnight at 20 °C before purification. The secreted furin was purified from the culture media using Ni-NTA agarose (Qiagen) affinity chromatography with gravity flow.

Enzymatic activity and inhibition assays

In brief, the activity of human furin was measured by a continuous kinetic assay, with the substrate Boc-Arg-Arg-Ala-Arg-AMC (GL Biochem) or Boc-Arg-Val-Arg-Arg-AMC (GL Biochem), using wavelengths of 360±40 nm and 460±40 nm for excitation and emission, respectively. Furin was added in assay buffer containing 100 mM HEPES buffer, pH 7.0, 0.2% (v/v) Triton X-100, 2 mM $CaCl_2$ and 0.1 mg/mL BSA. The assay started by immediately mixing with different concentrations of substrate (0.39-200 μM). The fluorophore, 7-amino-4-methylcoumarin (AMC) group released from Boc-RRAR-AMC or Boc-RVRR-AMC was monitored in the form of relative fluorescence units as a function of time (RFU/min) using a BioTEK Synergy H1 multimode microplate reader at 37 °C. The IC_{50} values were calculated by fitted regression equation using the-log plot (GraphPad Prism). Each value was expressed with the means ± SD of three independent tests, each with three replicates.

Supplemental References

Abagyan, R., Totrov, M., Kuznetsov, D. (1994). ICM-a new method for protein modeling and design-applications to docking and structure prediction from the distorted native conformation. J Comput Chem *15*, 488-506.

Dahms, S.O., Hardes, K., Steinmetzer, T., Than, M.E. (2018). X-ray Structures of the proprotein convertase furin bound with substrate analogue inhibitors reveal substrate specificity determinants beyond the S4 pocket. Biochemistry *57*, 925-934.

Irwin, J.J., Sterling, T., Mysinger, M.M., Bolstad, E.S., Coleman, R.G. (2012). ZINC: a free tool to discover chemistry for biology. J Chem Inf Model *52*, 1757-1768.
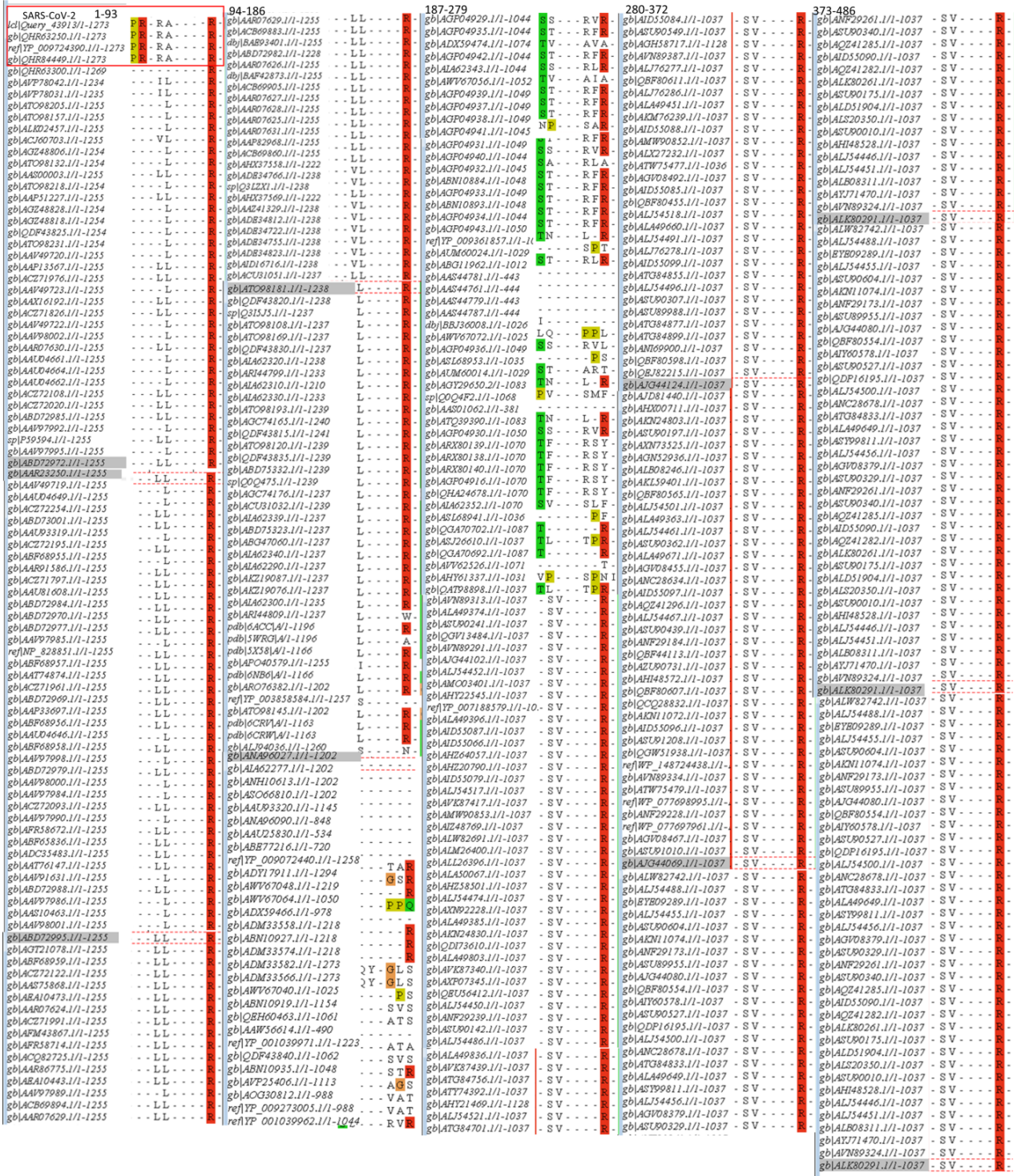
Figure S1. Multiple sequence alignment of 1000 Spike proteins(1-486). Related to Figure 1.
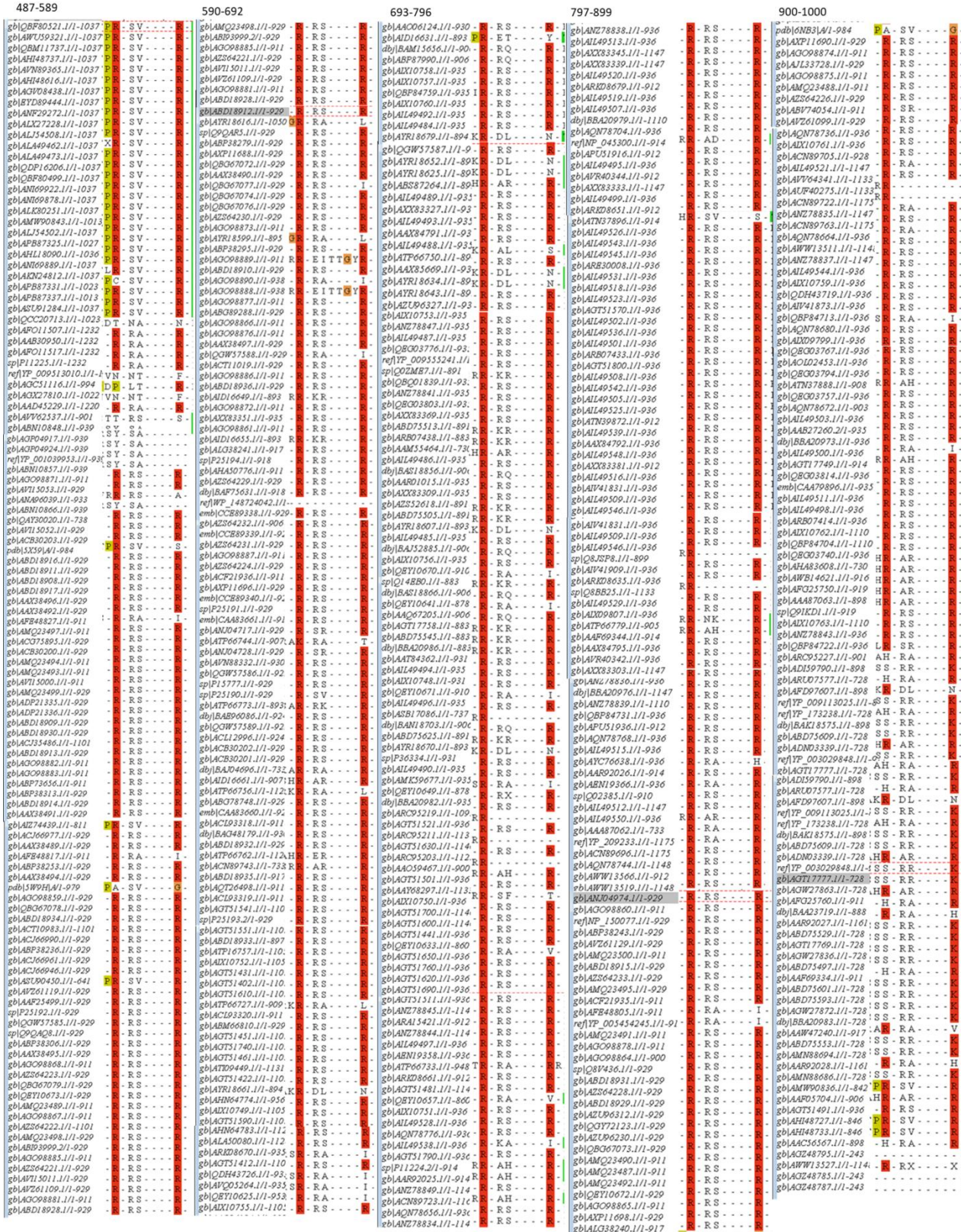
Figure S2. Multiple sequence alignment of 1000 Spike proteins(487-1000). Related to Figure 1.

```
Sequence    457    YLYRLFR|KS   0.179   .
Sequence    458    LYRLFRK|SN   0.100   .
Sequence    462    FRKSNLK|PF   0.069   .
Sequence    466    NLKPFER|DI   0.154   .
Sequence    509    VCYQPYR|VV   0.091   .
Sequence    528    ATVCGPK|KS   0.059   .
Sequence    529    TVCGPKK|ST   0.146   .
Sequence    535    KSTNLVK|NK   0.066   .
Sequence    537    TNLVKNK|CV   0.093   .
Sequence    557    VLTESNK|KF   0.057   .
Sequence    558    LTESNKK|FL   0.091   .
Sequence    567    PFQQFGR|DI   0.127   .
Sequence    577    DTTDAVR|DP   0.076   .
Sequence    634    QLTPTWR|VY   0.098   .
Sequence    646    SNVFQTR|AG   0.103   .
Sequence    682    TQTNSPR|RA   0.111   .
Sequence    683    QTNSPRR|AR   0.146   .
Sequence    685    NSPRRAR|SV   0.620   *ProP*
Sequence    733    LPVSMTK|TS   0.065   .
Sequence    765    FCTQLNR|AL   0.076   .
Sequence    776    IAVEQDK|NT   0.071   .
Sequence    786    EVFAQVK|QI   0.066   .
Sequence    790    QVKQIYK|TP   0.056   .
Sequence    795    YKTPPIK|DF   0.079   .
Sequence    811    ILPDPSK|PS   0.058   .
Sequence    814    DPSKPSK|RS   0.071   .
Sequence    815    PSKPSKR|SF   0.333   .
Sequence    825    EDLLFNK|VT   0.053   .
Sequence    835    ADAGFIK|QY   0.094   .
Sequence    847    LGDIAAR|DL   0.105   .
Sequence    854    DLICAQK|FN   0.064   .
Sequence    905    AMQMAYR|FN   0.169   .
Sequence    921    VLYENQK|LI   0.065   .
Sequence    933    FNSAIGK|IQ   0.067   .
Sequence    947    TASALGK|LQ   0.077   .
Sequence    964    ALNTLVK|QL   0.079   .
Sequence    983    LNDILSR|LD   0.068   .
Sequence    986    ILSRLDK|VE   0.129   .
Sequence    995    AEVQIDR|LI   0.081   .
```

ProP 1.0: predicted propeptide cleavage sites in Sequence, furin-specific prediction

Propeptide cleavage potential

Threshold
Signal peptide cleavage
Propeptide cleavage

Sequence position
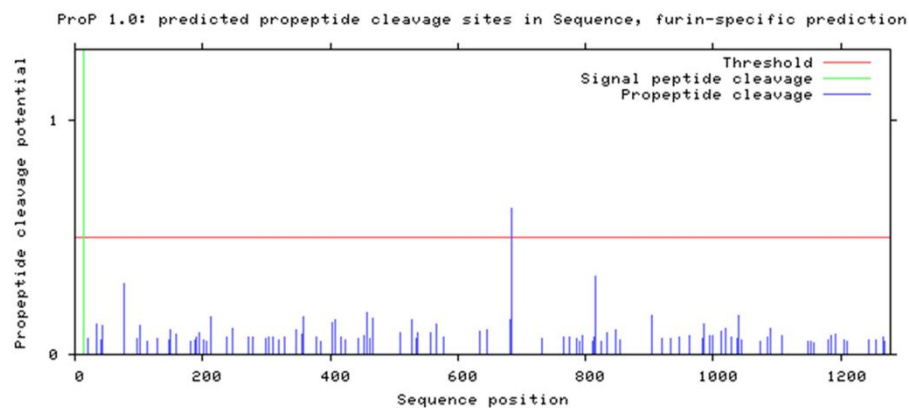
Figure S3. Result of furin cleavage site pridiction of Spike protein in SARS-CoV-2, which predicted by online method ProP 1.0 Server. Related to Table 1.
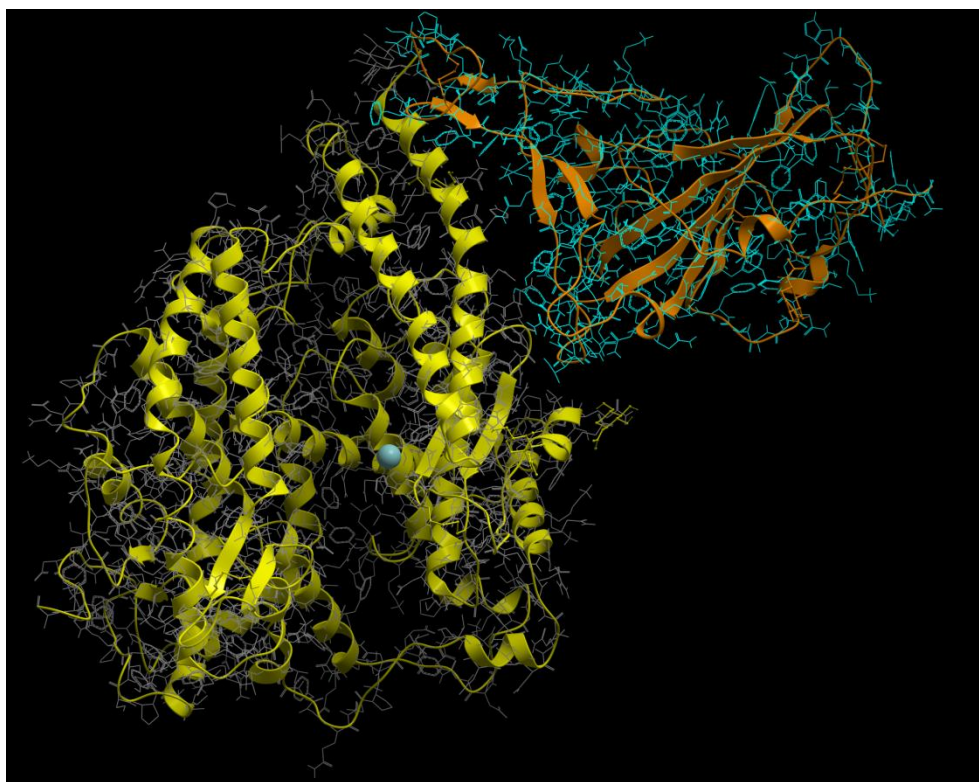
Fig S4 Protein-protein docking calculation model of SARS-CoV-2 spike RBD (light blue) with human ACE2 (yellow), original RBD conformation was shown in orange. The calculated free energy is -50.13 Kcal/mol. Related to Figure 3.
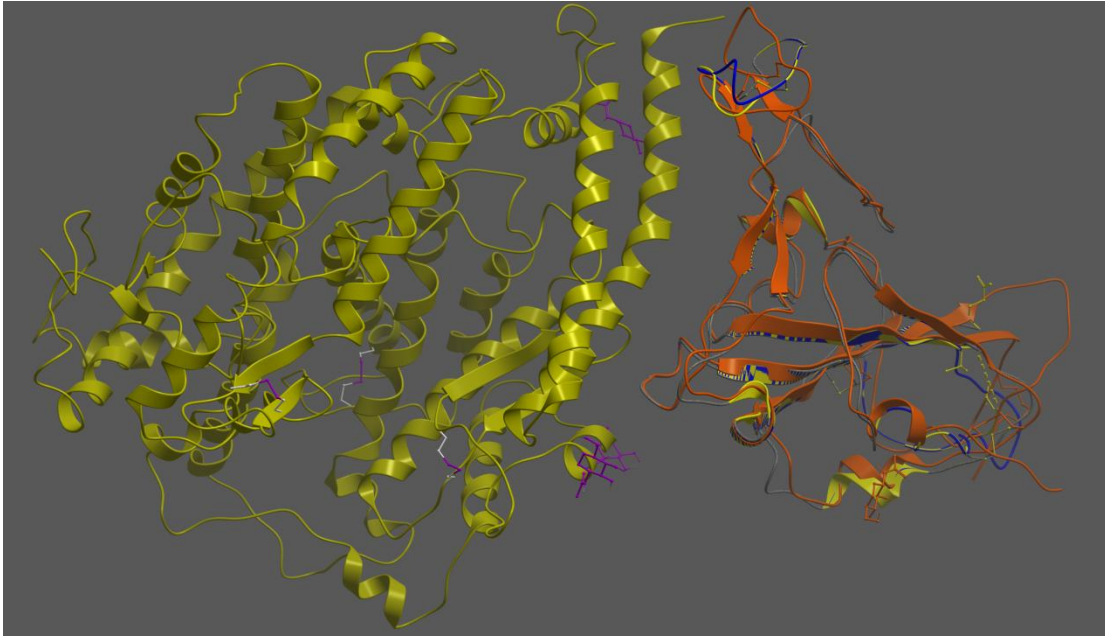
Fig S5 Comparison of SARS-CoV-2 spike RBD (orange) and SARS spike RBD (yellow). The complex with ACE2 (left part, yellow) was shown. The homology model of SARS-CoV-2 spike RBD built from SARS spike RBD was shown as blue. Related to Figure 3.
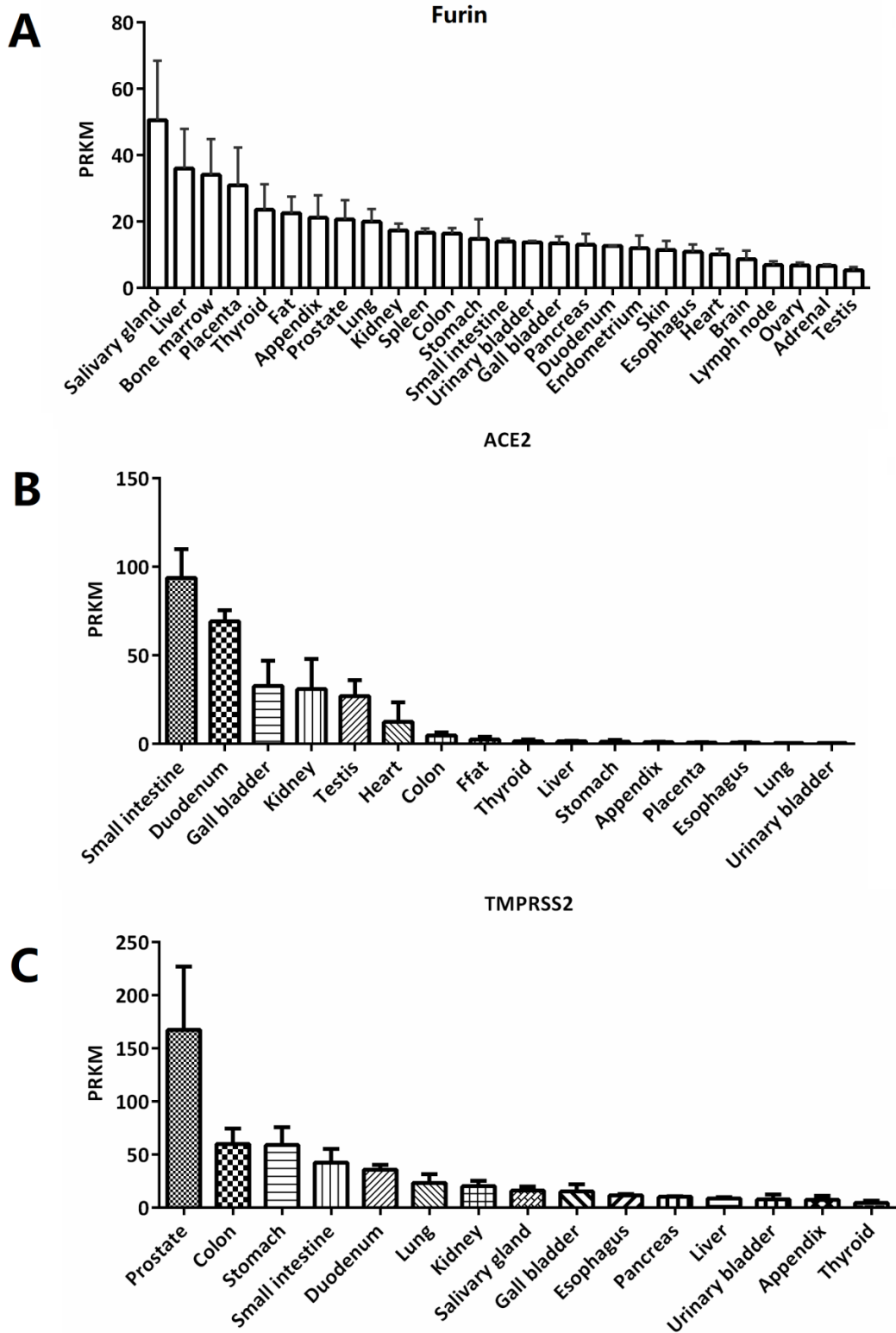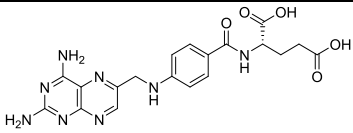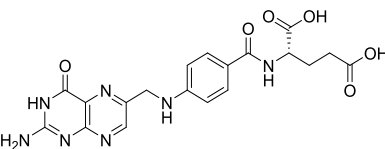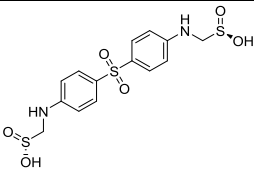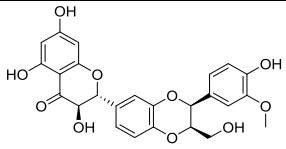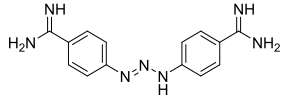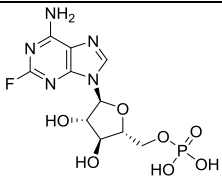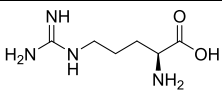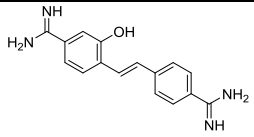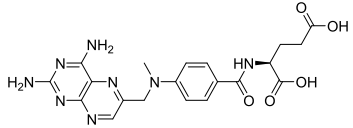
Figure S6. Expression levels of Furin, ACE2 and TMPRSS2 in various tissues. The data is from pubmed. Related to Figure 2B.

Table S1   Potential furin inhibitors from ZINC drug database, related to Figure 4

No.	Drug Name	Structure	Pharmacological functions
1	Aminopterin		Anti-tumor
2	Folic acid		Vitamin B9, necessary material for the growth and reproduction of body cells
3	Sulfoxone		Antibacterial effect
4	Silybin		Hepatoprotective effect
5	Diminazene		Insecticidal effect
6	Fludarabine phosphate		Anti-tumor
7	L-Arginine		Nutritional supplement
8	Hydroxystilbamidine		Antifungal effect
9	Methotrexate		Antineoplastic, antirheumatic effects
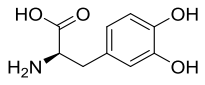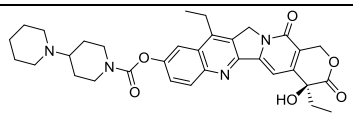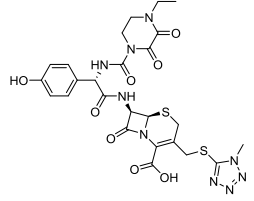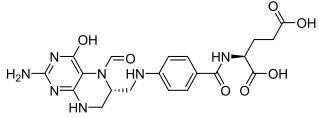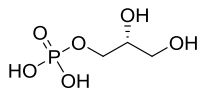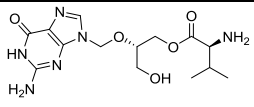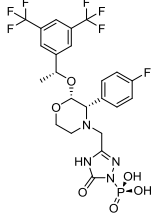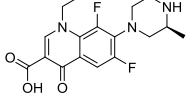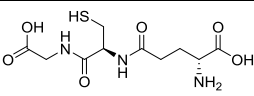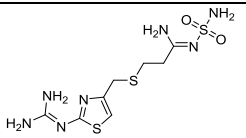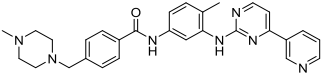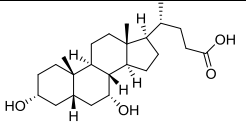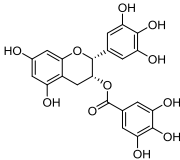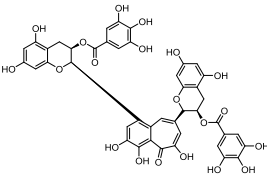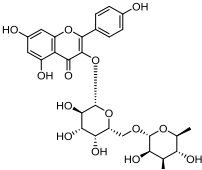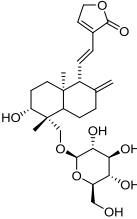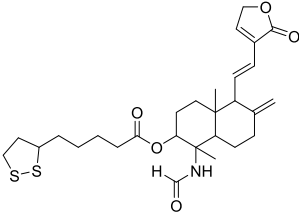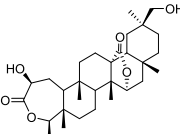
10	L-dopa		Treatment of Parkinson's disease
11	Irinotecan		Anti-tumor
12	Cefoperazone		Antibacterial effect
13	Folinic acid		Folic acid supplement
14	Glycerol 3-phosphate		Intermediate for serine synthesis
15	Valganciclovir		Antivirus
16	Fosaprepitant		Treatment of nausea and vomiting induced by chemotherapy
17	Lomefloxacin		Antibacterial effect
18	Glutathione		Hepatoprotective effect
19	Famotidine		Treatment of gastrohelcosis
20	Imatinib		Anti-tumor
21	Chenodeoxycholic acid		Dissolving gallstones

Table S2 Potential furin inhibitors from in-house natural product database, related to Figure 5

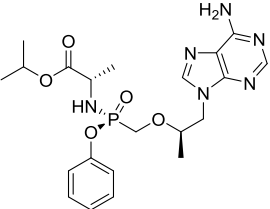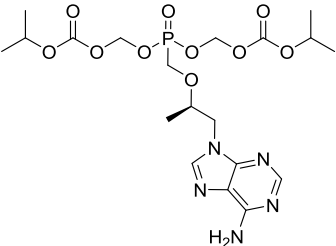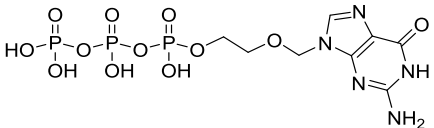| No.	Drug Name	Structure	Pharmacological functions	Source
1	(-)-Epigallocatechin gallate		Antioxidation, anti-tumor, treatment of depression	*Camellia sinensis*
2	Theaflavin 3,3'-di-*O*-gallate		Antioxidant effect, anti-tumor, anti-virus	*Camellia sinensis*
3	Biorobin		Anti-virus	*Ficus benjamina*
4	14-deoxy-11,12-didehydroandrographiside		Anti-virus, anti-inflammatory effect	*Andrographis paniculata*
5	(1*S*,2*R*,4a*S*,5*R*,8a*S*)-1-formamido-1,4a-dimethyl-6-methylene-5-((*E*)-2-(2-oxo-2, 5- dihydrofuran-3-yl)ethenyl) decahydronaphthalen-2-yl 5-((*R*)-1,2-dithiolan-3-yl) pentanoate		Anti-virus, anti-inflammatory effect	Andrographolide derivatives
6	2*β*,30*β*-dihydroxy-3,4-seco-friedelolactone-27-lactone		Anti-virus	*Viola diffusa*
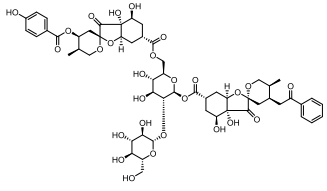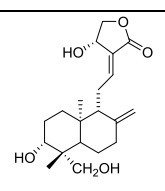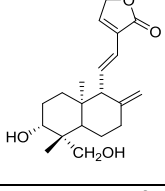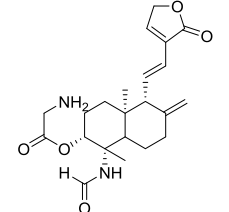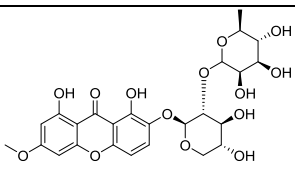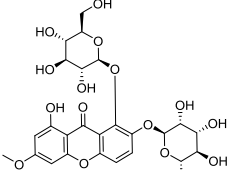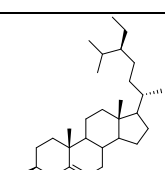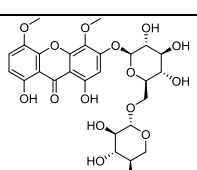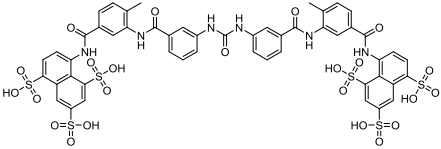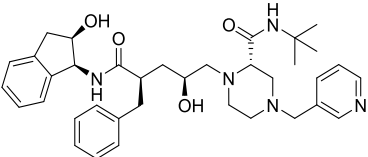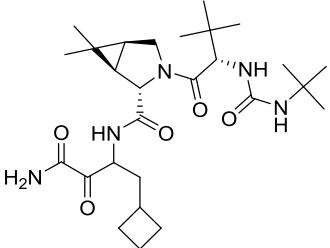
7	Phyllaemblicin G7		Anti-virus	*Phyllanthus emblica*
8	Andrographolide		Anti-virus, anti-inflammatory effect	*Andrographis paniculata*
9	14-deoxy-11,12-didehydroandrographolide		Anti-virus, anti-inflammatory effect	*Andrographis paniculata*
10	(1*S*,2*R*,4a*S*,5*R*,8a*S*)-1-formamido-1,4a-dimethyl-6-methylene-5-((*E*)-2-(2-oxo-2,5-dihydrofuran-3-yl)ethenyl) decahydronaphthalen-2-yl 2-aminoacetate		Anti-virus, anti-inflammatory effect	Andrographolide derivatives
11	2-[[2-*O*-(6-deoxy-*α*-L-mannopyranosyl)-*β*-D-xylopyranosyl]oxy]-1,8-dihydroxy-6-ethoxy-9*H*-xanthen-9-one		Anti-virus, anti-inflammatory effect	*Swertia kouitchensis*
12	Kouitchenside J		Anti-virus, anti-inflammatory effect	*Swertia kouitchensis*
13	Stigmast-5-en-3-ol		Antioxidant effect	*Spatholobus suberectus dunn*
14	Kouitchenside F		Anti-virus, anti-inflammatory effect	*Swertia kouitchensis*

Table S3

Potential furin inhibitors from the common antiviral drugs database, related to Figure 6

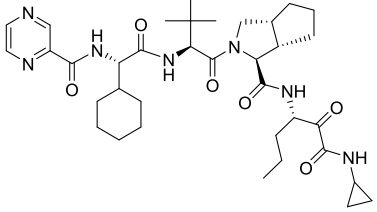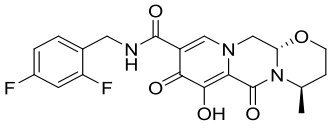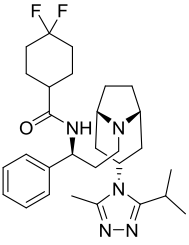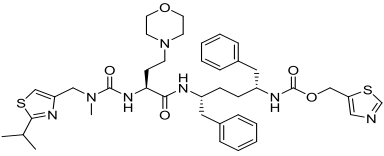| No.	Drug Name	Structure	Pharmacological functions
1	Suramin		DNA topoisomerase II inhibitor
2	Indinavir		Human immunodeficiency virus Protease (HIV PR), anti-malaria
3	Boceprevir		Hepatitis C virus Serine protease NS3/4A (HCV NS3/4A) Modulator
4	Tenofovir alafenamide		HIV-1, HBV nucleotide reverse transcriptase inhibitor
5	Tenofovir disoproxil		HIV, HBV nucleotide reverse transcriptase inhibitor
6	Acycloguanosine triphosphate		Thymidine kinase of herpesvirus
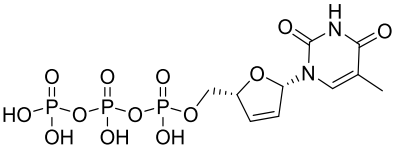
7	Telaprevir		Hepatitis C virus Serine protease NS3/4A (HCV NS3/4A) Modulator
8	Dolutegravir		Human immunodeficiency virus Integrase (HIV IN)
9	Maraviroc		1.C-C chemokine receptor type 5 (CCR5) 2.CCR5 messenger RNA(CCR5 mRNA)
10	Cobicistat		Inhibitor of cytochrome P450 3A (CYP3A) enzymes
11	Stavudine triphosphate		Nucleoside analogue reverse transcriptase inhibitor used in the treatment of HIV infection

Table S4. In vitro furin inhibitory effects of screening hits. Related to Figure 7.

Compounds name	In vitro furin protease inhibition percentage at 100μM(％)	IC50 (μM）
Aminopterin	72	>30
Folic acid	<30	>30
Sulfoxone	<30	>30
Silybin	74	>30
Diminazene	95	5.42 ±0.11
Fludarabine phosphate	<30	>30
L-Arginine	<30	>30
Hydroxystilbamidine	<30	>30
Methotrexate	73	>30
L-dopa	<30	>30
Irinotecan	<30	>30
Cefoperazone	<30	>30
Folinic acid	44	>30
Glycerol 3-phosphate	<30	>30
Valganciclovir	<30	>30
Fosaprepitant	<30	>30
Lomefloxacin	40	>30
Glutathione	<30	>30
Famotidine	<30	>30
Imatinib	58	>30
Chenodeoxycholic acid	<30	>30
Suramin	<30	>30
Indinavir	<30	>30
Boceprevir	<30	>30
Tenofovir alafenamide	<30	>30
Tenofovir disoproxil	38	>30
Acycloguanosine triphosphate	<30	>30
Telaprevir	<30	>30
Dolutegravir	<30	>30
Maraviroc	<30	>30
Cobicistat	<30	>30
Stavudine triphosphate	<30	>30
(-)-Epigallocatechin gallate	<30	>30

Theaflavin 3,3'-di-O-gallate	<30	>30
Biorobin	<30	>30
14-deoxy-11,12-didehydroandrographiside	<30	>30
Phyllaemblicin G7	<30	>30
Andrographolide	<30	>30
14-deoxy-11,12-didehydroandro grapholide	<30	>30
Kouitchenside J	<30	>30
Stigmast-5-en-3-ol	<30	>30
Kouitchenside F	<30	>30